CHAPTER IV
ISOTHERMAL MELT CRYSTALLIZATION AND MELTING BEHAVIOR FOR THREE LINEAR AROMATIC POLYESTERS

Nujalee Dangseeyun, Phornphon Srimoaon, Pitt Supaphol,* and Manit Nithitanakul

The Petroleum and Petrochemical College, Chulalongkorn University, Soi Chula 12, Phyathai Road, Pathumwan, Bangkok 10330, THAILAND

ABSTRACT

Isothermal crystallization and subsequent melting behavior of three different types of linear aromatic polyester, namely poly(ethylene terephthalate) (PET), poly (trimethylene terephthalate) (PTT), and poly(buthylene terephthalate) (PBT), were investigated (with an emphasis on PTT in comparison with PET and PBT). These polyesters were different in the number of methylene groups (i.e., 2, 3, and 4 for PET, PTT, and PBT, respectively). Isothermal crystallization studies were carried out in a differential scanning calorimeter (DSC) over the crystallization temperature range of 182 to 208°C. Wide-angle X-ray diffraction (WAXD) technique was used to obtain information about crystal modification and apparent degree of crystallinity. The kinetics of the crystallization process was assessed by a direct fitting of the experimental data to the Avrami, Tobin, Malkin and Urbanovici-Segal macrokinetic models. It was found that the crystallization rates of these polyesters were in the following order: PBT > PTT > PET, and the melting of these polyesters exhibited a multiple-melting phenomenon. Lastly, the equilibrium melting temperature of these polyesters was estimated based on the linear and non-linear Hoffman-Weeks extrapolative methods.

(**Key-words**: PET; PTT; PBT; crystallization kinetics; melting behavior)

---

* To whom correspondence should be addressed: Fax: +66-2215-4459; E-mail address: pitt.s@chula.ac.th

1. INTRODUCTION

In 1941, a new type of linear aromatic polyester, poly(trimethylene terephthalate) (PTT), was successfully synthesized by Whinfield and Dickson [1], but it was not commercially available then because of the expensiveness of 1,3-propanediol, one of the raw materials used to produce PTT. With a breakthrough in the synthesis of 1,3-propanediol at a much lower price, PTT is now commercially available and has been produced by Shell Chemicals under the tradename Corterra, joining the rank of other linear aromatic polyesters, poly(ethylene terephthalate) (PET) and poly(buthylene terephthalate) (PBT). PTT has properties in between those of PET and PBT, with an unusual combination of the outstanding properties of PET and processing characteristics of PBT. These make PTT highly suitable for uses in fiber, film and engineering thermoplastic applications.

PTT has three methylene units in its chemical structure, rendering PTT chains to be more flexible, hence greater crystallization rate, than those of PET. The glass transition and the apparent melting temperatures of PTT were reported by Huang and Chang [2] to be ca. 44 and 228°C, respectively. Like PET and PBT, PTT crystallizes into triclinic crystal structure, with the periodicity along the *c*-axis containing two repeating units and the methylene groups being arranged in a highly contracted gauche-gauche conformation [3].

Recently, Chuah [4] studied the overall crystallization kinetics of PTT based on the Avrami proposition. He found that, at a given degree of undercooling, the crystallization rate of PTT lies between those of PET and PBT. He reported that PBT has the highest crystallization rates with the Avrami rate constant (k_a) being in the order of 10^{-2} to 10^{-1} min^{-n}, which is approximately an order of magnitude greater than PTT at 10^{-3} to 10^{-2} min^{-n}, which, in turn, is about an order of magnitude faster than PET at 10^{-4} to 10^{-2} min^{-n}. Similar results were also reported by Huang and Chang [2].

The multiple melting phenomenon upon subsequent melting of isothermally crystallized PTT samples in a differential scanning calorimeter (DSC) was recently reported by Chung *et al.* [5]. They contributed the phenomenon to the dual populations of lamellar stacks formed during primary crystallization and recrystallization during subsequent heating process. They also reported, based on

wide-angle X-ray diffraction (WAXD) results, that the crystal modification of PTT does not change with crystallization temperature, at least within the temperature range studied [5].

In this manuscript, we report the overall isothermal crystallization and subsequent melting behavior of PTT in critical comparison with those of PET and PBT, based mainly on results obtained from DSC and WAXD techniques. The isothermal crystallization data are analyzed and described based on various mathematical models, namely the Avrami, Tobin, Malkin and Urbanovici-Segal macrokinetic models. The equilibrium melting temperatures of PTT, PET and PBT are also evaluated based on both linear and non-linear Hoffman-Weeks extrapolations.

2. Theoretical Background

Isothermal bulk crystallization kinetics of semicrystalline polymers in a DSC is usually studied by following the crystallization exotherms [6-7], based on the assumption that the evolution of crystallinity is linearly proportional to the evolution of heat released during the course of crystallization. Based on this notion, the relative crystallinity as a function of time $\theta(t)$ can be obtained according to the following equation:

$$\theta(t) = \frac{\int_0^t \left(\frac{dH_c}{dt}\right) dt}{\int_0^\infty \left(\frac{dH_c}{dt}\right) dt} \in [0,1] \qquad (1)$$

where t and ∞ are the elapsed time during the course of crystallization and at the end of crystallization process, respectively, and dH_c is the enthalpy of crystallization released during and infinitesimal time interval dt.

In order to quantitatively describe the macroscopic evolution of crystallinity during primarily crystallization under quiescent isothermal conditions, a number of macrokinetic models have been proposed over the past sixty years. They are, for examples, the so-called 'Avrami' [8-13], the Tobin [14-16], the Malkin [17], and the Urbanovici-Segal [18] models. In Avrami model [8-13], the relative crystallinity as

a function of time $\theta(t)$ is related to the crystallization time t according to the equation:

$$\theta(t) = 1 - \exp\left[-(K_a t)^{n_a}\right] \in [0,1] \qquad (2)$$

where K_a and n_a are the Avrami crystallization rate constant and the Avrami exponent, respectively. Usually, the Avrami rate constant K_a is written in the form of the composite Avrami rate constant k_a (i.e. $k_a = K_a^n$). It was shown that k_a (the dimension of which is given in $(\text{time})^{-n}$) is not only a function of temperature, but also a function of the Avrami exponent n_a [19]. As a result, use of K_a should be more preferable than use of k_a due partly to the facts that it is independent of the Avrami exponent n_a and its dimension is given in $(\text{time})^{-1}$. It should be noted that both K_a and n_a are constants specific to a given crystalline morphology and type of nucleation for a particular crystallization condition [20] and that based on the original assumptions of the theory, the value of the Avrami exponent n_a should be an integer ranging from 1 to 4.

Aiming at improving the Avrami equation in describing the experimental data at the later stages of crystallization, Tobin [10-12] proposed a different expression to describe the kinetics of phase transformation by taking into account the growth impingement. The original theory was written in the form of a nonlinear Volterra integral equation, of which the zeroth order solution is given by:

$$\theta(t) = \frac{(K_t t)^{n_t}}{1 + (K_t t)^{n_t}} \in [0,1] \qquad (3)$$

where K_t is the Tobin rate constant, and n_t the Tobin exponent. Based on this proposition, the Tobin exponent needs not be integral [14-16], and it is mainly governed by different types of nucleation and growth mechanisms. It should be noted that, according to the original applications [14-16], the Tobin rate constant is written in the form of the composite Tobin rate constant k_t (i.e. $k_t = K_t^n$), which is not only a function of time, but also a function of the Tobin exponent n_t (similar to the case of k_a mentioned previously) [19]. As a result, use of K_t should be more preferable than use of k_t due partly to the facts that it is independent of the Tobin exponent n_t and its dimension is given in $(\text{time})^{-1}$.

Derived based on a postulation that the overall crystallization rate equals the summation of the rate at which the degree of crystallinity varies with the emergence of primary nuclei and the rate of variation in the degree of crystallinity varies with crystal growth rate, Malkin *et al.* [17] arrived at a totally different kinetic equation:

$$\theta(t) = 1 - \frac{C_0 + 1}{C_0 + \exp(C_1 t)} \in [0,1] \qquad (4)$$

where C_0 is the Malkin exponent which relates directly to the ratio of the crystal growth rate G to the primary nucleation rate I (i.e. $C_0 \propto G/I$), and C_1 is the Malkin crystallization rate constant which relates directly to overall crystallization (i.e. $C_1 = aG+bI$, where a and b are some specific constants). It should be noted that the dimension of the Malkin rate constant is given in $(\text{time})^{-1}$.

Recently, Urbanovici and Segal [18] proposed a new macrokinetic equation, which is essentially a generalization of the Avrami model. In this proposition, the relation between the relative crystallinity as a function of time $\theta(t)$ and the crystallization time t is written as:

$$\theta(t) = 1 - \left[1 + (r-1)\left(K_{us} t^{n_{us}}\right)\right]^{1/(1-r)} \in [0,1] \qquad (5)$$

where K_{us} and n_{us} are the Urbanovici-Segal crystallization rate constant and the Urbanovici-Segal exponent, respectively. r is the parameter satisfying the condition $r > 0$. At the condition where $r \rightarrow 1$, the Urbanovici-Segal model becomes identical to the Avrami model [18]. This simply means that parameter r merely the factor determining the degree of deviation of the Urbanovici-Segal model from the Avrami model. It is worth noting that both K_{us} and n_{us} have similar physical meanings to the Avrami kinetic parameters (i.e. K_a and n_a), and the dimension of K_{us} is also given in $(\text{time})^{-1}$.

3. EXPERIMENTAL DETAIL

3.1. Materials

Poly(trimethylene terephthalate) (PTT) was supplied in pellet form by Shell Chemicals (USA) (Corterra CP509201). The weight- and number-average molecular weights of this resin were determined to be ca. 78,100 and 34,700 Daltons, respectively. Poly(ethylene terephthalate) (PET) was supplied in pellet form by Indo

PET (Thailand) (N1). The weight- and number-average molecular weights of this resin were determined to be ca. 84,500 and 41,200 Daltons, respectively. Finally, poly(buthylene terephthalate) (PBT) was supplied in pellet form by LG Chem (Korea) (LUPOX GP-2000). The weight- and number-average molecular weights of this resin were determined to be ca. 71,500 and 36,300 Daltons, respectively. It should be noted that molecular weight characterization of these resins was carried out by Dr. Hoe H. Chuah and his co-workers of Shell Chemicals (USA) based on size-exclusion chromatography (SEC) technique.

3.2. Sample Preparation

PET, PTT and PBT resins were dried in a vacuum oven at 140°C for 5 hours prior to further use. Films of approximately 200 μm in thickness was melted-pressed at 280°C for PET and 260°C for PTT and PBT in a Wabash V50H compression molding machine under an applied pressure of 4.62×10^2 $MN\cdot m^{-2}$. After 5 min holding time, the films were taken out and allowed to cool, under the ambient condition, down to room temperature between the two metal platens. This treatment assumes that previous thermo-mechanical history was essentially erased, and provided a standard crystalline memory condition for the as-prepared film.

3.3. Differential Scanning Calorimetry Measurements

A DSC (DSC-7, Perkin-Elmer) was used to record isothermal crystallization exotherms and subsequent melting endotherms of these polyester resins. Calibration for the temperature scale was carried out using a pure indium standard (T_m^o= 156.6° C and ΔH_f^o = 28.5 $J\cdot g^{-1}$) on every other run to ensure accuracy and reliability of the data obtained. To minimize thermal lag between polymer sample and DSC furnace, each sample holder was loaded with a disc-shape sample weighing around 8.0 ± 0.5 mg which was cut from the as-prepared films. It is worth noting that each sample was used only once and all the runs were carried out under nitrogen atmosphere to prevent extensive thermal degradation.

The experiment started with heating each sample from 40°C at a heating rate of 80°C min^{-1} to a desired fusion temperature T_f (i.e., at 280°C for PET and 260°C for PTT and PBT respectively). To ensure complete melting, the sample was kept at the

respective T_f for a holding period of 5 min. After this period, each sample was rapidly cooled (i.e., ca. 200°C min^{-1}) from T_f to a desired crystallization temperature, where it was held to the completion of the crystallization process (achievable when no significant change in the heat flow as a function of time was further observed). Both the isothermal crystallization exotherms and subsequent melting endotherms were recorded for further analysis. The heating rate used to record all of the subsequent melting endotherms was 10°C min^{-1}. The kinetics of the isothermal crystallization process was carried out by directly fitting the experimental data to the aforementioned macrokinetic models.

3.4. Crystal Structure and Crystallinity Measurements

Wide-angle X-ray diffraction (WAXD) technique was employed to determine crystal modification and apparent degree of crystallinity of PTT samples prepared in the same conditions set forth for samples prepared for the DSC measurements (viz. after the samples were completely crystallized at a desired crystallization temperature, they were immediately quenched, without subsequent heating, to 30°C). Each sample was then taken out of the DSC sample holder and was pasted onto a glass X-ray sample holder, using vasaline as adhesive. The WAXD intensity pattern of each sample was then collected on a Rigaku Rint 2000 diffractometer, equipped with a computerized data collection and analytical tools. The X-ray source (CuKα radiation, λ = 1.54 Å) was generated with an applied voltage of 40 kV and a filament current of 30 mA.

4. RESULTS AND DISCUSSION

4.1. Isothermal Crystallization of Polyesters from the Melt

Figure 1 illustrates the time-dependent relative crystallinity function $\theta(t)$ (after subtraction of the induction period t_0) of PTT samples crystallized at two different temperatures (i.e., 184 and 194°C, respectively). It should be noted that the raw data are shown in Figure 1 as different geometrical points. Evidently, within the temperature range studied, the time to reach the ultimate crystallinity (i.e., complete crystallization) increased with increasing crystallization temperature T_c. An

important bulk or overall crystallization kinetic parameter which can be determined directly from the $\theta(t)$ data is the half-time of crystallization $t_{0.5}$, defined as the elapsed time from the onset of crystallization to the point where the crystallization is half-completed. Table 1 summarizes the values of crystallization half-time $t_{0.5}$ taken from all of the experimental data obtained.

According to Table 1, it is apparent that, for each polymer, the half-time of crystallization $t_{0.5}$ increased exponentially with increasing crystallization temperature T_c, at least within the range of crystallization temperatures studied. Comparison of crystallization kinetics among these polyesters, which have different practical crystallization windows over the absolute temperature scale (i.e., $T_g < T_c < T_m^o$), can be carried out by plotting the kinetic parameters versus degree of undercooling ΔT, defined as the difference between the equilibrium melting temperature T_m^o and the crystallization temperature T_c (i.e., $\Delta T = T_m^o - T_c$). It should be noted that the degree of undercooling designates the driving force for crystallization. In this manuscript, the value of the equilibrium melting temperature T_m^o for PET, PTT, and PBT were determined by the linear Hoffman-Weeks extrapolation to be 270.1, 243.6, and 235.4°C, respectively (for detailed discussion on the determination of the equilibrium melting temperature, please refer to the appropriate section later in this manuscript).

Figures 2 and 3 show, respectively, the half-times of crystallization $t_{0.5}$ and its inversed values (i.e., the reciprocal half-times of crystallization $t_{0.5}^{-1}$) versus degree of undercooling for all three polyesters studied. It should be noted that such a plot of the reciprocal half-time of crystallization versus degree of undercooling is regarded as the most fundamental representation of the bulk crystallization rate of a semi-crystalline polymer. Considering Figure 2, it is evident that all of the polymers studied exhibited decreased crystallization half-time with increasing degree of undercooling (or with decreasing crystallization temperature). In general, for a given degree of undercooling, PBT exhibited the lowest $t_{0.5}^{-1}$ value, followed by that of PTT and PET, respectively. The results clearly suggested that crystallization proceeded at a much faster rate with increasing degree of undercooling (or with decreasing crystallization temperature) and that PBT crystallized the fastest, followed PTT and PET, respectively.

The above conclusion can be drawn much easier if one considers Figure 3. it is evident that all of the polymers studied exhibited increased reciprocal half-time with increasing degree of undercooling (or with decreasing crystallization temperature). For examples, at $\Delta T = 50$ K, the reciprocal half-times of crystallization for PBT, PTT, and PET were 2.63, 0.743, and 0.0978 min^{-1}, respectively. This clearly confirmed that PBT exhibited the highest crystallization rate, followed respectively by PTT and PET. For a qualitative comment on the data obtained, it should be noted that, in the case where $t_{0.5}$ data can be measured accurately over the whole temperature range in which polymers can crystallize (i.e., $T_g < T_c < T_m^o$), the plot of the reciprocal half-time of crystallization versus either crystallization temperature or degree of undercooling is expected to exhibit the typical bell-shaped curve, which is characterized by the nucleation-controlled character at "high" crystallization temperatures or low degrees of undercooling and the diffusion-controlled one at "low" crystallization temperatures or high degrees of undercooling. According to this notion, the results shown in Figure 3 suggested that all of the polymers crystallized within the nucleation-controlled region.

4.2. Isothermal Crystallization Kinetics based on the Avrami Analysis

The analysis based on the Avrami model can be done by fitting the $\theta(t)$ function obtained for each crystallization temperature to Equation (1). The Avrami exponent n_a and the Avrami rate constant K_a, provided by the program, are summarized in Table1. The exponent n_a for primary crystallization process was found to range from 1.64 to 2.05 for PET, 1.75 to 2.39 for PTT, and 1.63 to 2.24 for PBT, respectively. This may correspond to a two dimensional growth with a combination of thermal and athermal nucleation (as a result of the fractional n_a values observed) [20]. Intuitively, the temperature dependence of the exponent n_a, within the nucleation-controlled region, should be such that n_a decreases with decreasing crystallization temperature. This may be explained based on the fact that the number of athermal nuclei increased tremendously as the temperature decreased [21]. In other words, as the crystallization temperature decreases, the number of athermal nuclei that become stable at that temperature also increased, resulting in the

nucleation mechanism becoming more instantaneous in time and causing the Avrami exponent n_a to decrease.

According to Table 1, the crystallization rate constant K_a exhibited strong sensitivity to changes in the crystallization temperature, in that it increased with decreasing crystallization temperature (or with increasing degree of undercooling). This observation only holds true when the temperature is in the range in which nucleation is the rate determining factor. For the reciprocal half-times of crystallization $t_{0.5}^{-1}$ as a function of degree of undercooling of these polyesters, they also increased with decreasing crystallization temperature (or with increasing degree of undercooling). Indeed, the Avrami rate constant K_a can be calculated directly from the reciprocal half-time value (i.e., $K_a^*=(\ln 2)^{1/n_a}(t_{0.5}^{-1})$), in which the calculated rate constant values K_a^* are also listed for comparison in Table 1. Obviously, there is good agreement between the rate constant obtained from the fitting K_a and that obtained from the calculation K_a^*, with the calculated value being ca. 0.73% less than the experimental values on average for PTT.

Verification of the applicability and reliability of the fitting procedure used to describe the isothermal crystallization data of these polyesters can be performed by comparison of the Avrami kinetic parameters provided by the program to the ones obtained based on the traditional method (i.e., plot of $\ln[-\ln(1-\theta(t))]$ versus $\ln t$; where n_a = slope and $\ln k_a$ is the intercept on the y-axis: these values are listed in Table 1.as n_a^{**} and K_a^{**}, respectively). It should be noted that the experimental data $\theta(t)$ used to fit the linear least square line were in the range of 0.1 to 0.8. Apparently, extremely good agreement of the kinetic parameters obtained from the two different methods is realized. This suggests that the fitting method can be used to analyze the isothermal crystallization data of these polyesters with a high level of confidence.

4.3. Isothermal Crystallization Kinetics based on the Tobin Analysis

The analysis based on the Tobin model can be performed by fitting the $\theta(t)$ function obtained for each crystallization temperature to Equation (3). Table 2 summarizes the Tobin kinetic parameters n_t and K_t, as well as the r^2 parameter. The Tobin exponent n_t for primary crystallization was found to range from 2.55 to 3.47

for PET, 3.06 to 3.78 for PTT, and 2.46 to 3.85 for PBT. By comparison, it is apparent that, at an arbitrary crystallization temperature, the Avrami exponent n_a is consistently lower in value than the Tobin exponent n_t. By taking the average value of the difference between the two values, we are able to conclude, based on our experimental observation, that $n_t \approx n_a + 1.3$, which is in general accordance with observations by other researchers [22,23].

According to Table 2, the Tobin rate constant K_t clearly exhibited a similar trend to that of the Avrami rate constant K_a in that it is greater in its value at low crystallization temperatures than that at high temperatures. According to Equation 3, the Tobin rate constant can also be calculated from the reciprocal half-time value $t_{0.5}^{-1}$ (i.e., $K_t^* = t_{0.5}^{-1}$). The calculated values K_t^* are also listed in Table 2. The discrepancy between the average value of rate constant obtained from the fitting K_t and that obtained from the calculation K_t^* of 1.89% for PTT was found, as opposed to around 0.73% difference in K_a and K_a^* values for PTT. PET and PBT also showed similar trends. This suggests that the experimental data of these polyesters can be fitted to the Avrami model better than to the Tobin one. This can also be confirmed based on the fact that the r^2 values listed in Table 1 are much greater than those listed in Table 2, indicating the much better fitting performance of the Avrami model.

4.4. Isothermal Crystallization Kinetics Based on the Malkin Analysis

The analysis based on the Malkin model can be carried out by fitting the $\theta(t)$ function obtained for each crystallization temperature to Equation (4). The kinetic parameters specific to the Malkin model C_0 and C_1, as well as r^2 parameter, are listed in Table 3. The C_0 parameter was found to range from 4.55 to 25.74 for PET, 7.01 to 28.01 for PTT and 4.56 to 17.39 for PBT.

Unlike the Avrami and the Tobin models, there is no direct analytical procedure for the determination of the Malkin kinetic parameters. Since, fundamentally, the Malkin exponent C_0 is related directly to the Avrami exponent n_a according to the following expression [17]:

$$C_0 = 4^{n_a} - 4 \qquad (6)$$

It should exhibit a similar temperature dependence to that of Avrami exponent n_a. According to Table 3, the Malkin rate constant C_1 also exhibited a temperature dependence in a similar fashion as the crystallization rate constants characteristic of both the Avrami and Tobin models. This is not surprising since the Malkin rate constant C_1 relates to the Avrami kinetic parameters (i.e., n_a and k_a) according to the following expression [17]:

$$C_1 = \frac{\ln(4^{n_a} - 2)K_a}{(\ln 2)^{n_a}} \tag{7}$$

The estimated Malkin kinetic parameters are also listed in Table 4, in which they are denoted C_0* and C_1*, respectively. Evidently, the estimated rate constant C_1* was found to be in good agreement with that obtained from the direct fitting method C_1. Like the other two rate constants, the Malkin rate constant C_1 can also be calculated directly from the reciprocal half-time $t_{0.5}^{-1}$ (i.e., $C_1 = \ln(4^{n_a} - 2)(t_{0.5}^{-1})$). Although not listed in Table 3, the C_1 values calculated from $t_{0.5}^{-1}$ values are found to be almost identical to the estimated Malkin crystallization rate values C_1*.

4.5. Isothermal Crystallization Kinetics based on the Urbanovici-Segal Analysis

Analogous to the previous three cases, data analysis based on the Urbanovici-Segal kinetic equation is carried out by directly fitting the experimental $\theta(t)$ data obtained for each crystallization temperature to Equation (5). Table 4 summarizes the Urbanovici-Segal kinetic parameters (i.e., n_{us}, K_{us} and r) along with the r^2 parameter obtained with the best fit. Accordingly to Table 4, the Urbanovici-Segal exponent n_{us} was found to range from 1.59 to 2.87 for PET, 1.78 to 2.43 for PTT, and 1.5 to 2.21 for PBT. The Urbanovici-Segal rate constant K_{us} apparently exhibited a similar trend to that suggested by the other crystallization rate parameters in that it decreased with increasing crystallization temperature (or with decreasing degree of undercooling). Like the Avrami rate constant K_a, the Urbanovici-Segal rate constant K_{us} can be calculated directly from the reciprocal half-time of crystallization $t_{0.5}^{-1}$ according to the following equation:

$$K_{us} = \left(\frac{0.5^{(1-r)} - 1}{r - 1}\right)^{1/n_{us}} t_{0.5}^{-1} \tag{8}$$

The calculated values of the Urbanovici-Segal rate constant (i.e., denoted K_{us}*) are also summarized in Table 4 for comparison. Evidently, extremely good agreement is observed between the experimental rate constant K_{us} and the calculated rate constant K_{us}* for PTT, with the calculated values being ca. 0.21% less than the experimental value on average.

Comparison between the kinetic parameters obtained from the Avrami and Urbanovici-Segal models (see Tables 1 and 4, respectively) indicates that the extent of discrepancy between the Urbanovici-Segal and Avrami kinetic parameters depended significantly on the value of the parameter r obtained. It was stated elsewhere in this manuscript that the Urbanovici-Segal model becomes identical to Avrami model when r approaches 1 [18]. According to Tables 1 and 4, when $r > 1$, the values of the Urbanovici-Segal kinetic parameters are systematically greater than those of Avrami ones, and the greater the value of r is from 1, the larger the discrepancy between the values of Urbanovici-Segal and Avrami kinetic parameters become. It is apparent according to Tables 1 and 4 that, when $r = 1.01$ (cf. PTT at T_c = 208°C), the difference between n_{us} and n_a was only 0.4% and that between K_{us} and K_a was only 0.9%; whereas, when $r = 1.10$ (cf. PTT at T_c = 198°C), the qualitative difference between n_{us} and n_a was as much as 5% and that between K_{us} and K_a was as much as 2.58%. On the contrary, when $r < 1$, the values of the Urbanovici-Segal kinetic parameters were systematically less than those of the Avrami ones.

4.6. Qualitative Comparison among the Four Macrokinetic Models

The quality of each macrokinetic equation in describing the experimental data $\theta(t)$ is quantitatively represented by the r^2 parameter obtained along with the best fit, in which the greater the value, the better the quality of the fit. Comparison of the values of the r^2 parameter summarized in Tables 1, 2, 3 and 4 indicates that the Avrami, Malkin and Urbanovici-Segal models gave very good description to the experimental data, while the Tobin model was not satisfactory in describing the experimental data. Graphically, deviation of the fits according to the Malkin and Tobin models (shown in Figure 1 as dashed and dash-dot lines, respectively) from the experimental data (shown in Figure 1 as different geometrical points) is obvious,

while that according to the Avrami and Urbanovici-Segal models (shown in Figure 1 as solid and dotted lines) from the experimental data is much less pronounced.

4.7. Further Discussion on the Temperature-Dependence of the Kinetic Paramters

Figure 4 illustrates the variation of all of the kinetic exponents of time (i.e., n_a, n_t, C_0 and n_{us}) along with the parameter r as a function of crystallization temperature (only shown for PTT). Apparently, the values of n_a, n_t, n_{us}, and r changed a little with, while C_0 was a bit more sensitive to, changes in the crystallization temperature. The kinetic exponents of time for PET and PBT also exhibited similar temperature dependency. Figure 5 exhibits the variation of all of the bulk crystallization rate parameters (i.e., $t_{0.5}^{-1}$, K_a, K_t, C_1, and K_{us}) as a function of crystallization temperature (only shown for PTT). It is apparent from Figure 5 that all of the bulk crystallization rate parameters exhibited a similar temperature-dependence. This similarity is understandable when one considers the fact that the units of these rate parameters were identical (i.e., min^{-1}) and that all of the crystallization rate parameters relate, in one way or another, to the reciprocal half-time of crystallization $t_{0.5}^{-1}$.

It is well accepted [19,23] that the bulk crystallization rate parameters (e.g., $t_{0.5}^{-1}$, K_a, K_t, C_1, and K_{us}) relate, in one way or another, to the primary nucleation rate I and/or the subsequent crystal growth rate G [24,25]: the temperature-dependence of the bulk rate parameters can accordingly be quantified and described. Even though the temperature-dependence of the parameters I and G are known to have a different temperature-dependence [24,25], the bulk crystallization rate parameters have often been taken to have a similar temperature dependence to that of the subsequent crystal growth rate G (written in the context of the original Lauritzen-Hoffman secondary nucleation theory (LH theory) [20,24]), which can be expressed as

$$\psi(T_c) = \psi_0 \exp\left(- \frac{A}{R(T_c - (T_g - C))} - \frac{B}{T_c(\Delta T)f} \right) \qquad (9)$$

where $\psi(T_c)$ and ψ_0 are the respective crystallization rate parameters (i.e. $t_{0.5}^{-1}$, K_a, K_t, C_1, and K_{us}) and the respective pre-exponential parameters (i.e. $(t_{0.5}^{-1})_0$,$K_{a,0}$, $K_{t,0}$, $C_{1,0}$, and $K_{us,0}$), respectively. A is a parameter relating to the activation energy which

characterizes molecular diffusion across the interfacial boundary between melt and crystals, while B is a parameter relating to the activation energy for the formation of the secondary nuclei. T_g is the respective glass transition temperature (i.e., $T_g \approx 78.0$, 44.0 and 34.7°C for PET, PTT, and PBT, respectively), T_g - C is the temperature where the cessation of long range molecular motion is expected and is often taken to be either ca. 30 or 50 K below the glass transition temperature, R is the universal gas constant, ΔT is the degree of undercooling (i.e., $\Delta T = T_m^o - T_c$; where $T_m^o \approx 270.1$, 243.6, and 235.4°C for PET, PTT, and PBT, respectively), and finally f is the factor used to correct for the temperature dependence of the heat of fusion (i.e., $f = 2T_c/(T_c + T_m^o)$).

Via the use of Equation (9), the temperature-dependent crystallization rate function $\psi(T_c)$ can be determined by fitting each respective crystallization rate parameter (i.e., $t_{0.5}^{-1}$, K_a, K_t, C_1, and K_{us}) collected at various crystallization temperatures to Equation (9). In order to obtain the best possible fits for the rate parameters with Equation (9), the value of the parameter C was chosen to be either 30 or 50 K, while those of T_g and T_m^o were fixed as previously noted. In so doing, the only unknown parameters which are provided by the program along with the best fits are ψ_0, A and B. Plots of the crystallization rate parameter of interest (i.e., $t_{0.5}^{-1}$, K_a, K_t, C_1, and K_{us}) and its corresponding best fit are illustrated in Figure 5., while the values of the fitting parameters are summarized in Table 5. It should be noted that all of the data used to fit to Equation (9) were in regime III (according to the context of the Lauritzen-Hoffman secondary nucleation theory [24,25]) for each polyester. The complication that arises from change in regimes can be ignored as long as the temperature range of interest is lower than the respective transition temperature from regime III to II (i.e., $T_{III \rightarrow II} \approx 194$°C [2] for PTT and 210°C for PBT [26], respectively). Examination of the values of the r^2 parameter listed in Table 5 suggests to us that the goodness of the fits of these parameters according to Equation (9) was very satisfactory. Specifically, it can be concluded that the quality of the fits, when using C = 30 K, was, in general, better than those, when using C = 50 K for PET and PTT. On the other hand, use of C = 50 K was the better in the case of PBT.

4.8. Crystal Modification and Crystallinity of PTT

In order to observe the crystal structure and the resulting apparent degree of crystallinity of PTT samples crystallized at different isothermal temperatures, WAXD technique was used. Figure 6 shows WAXD patterns of PTT samples crystallized at isothermal temperatures ranging from 182 to 206°C (each sample was prepared in DSC cell by quenching to 30°C, without subsequent melting, after complete crystallization at each respective temperature). Obviously, each samples exhibited seven characteristics peaks at the scattering angles 2θ of ca. 15.3, 16.8, 19.4, 21.8, 23.6, 24.6, and 27.3°, corresponding to the reflection planes of $(010), (0\bar{1}2), (012), (10\bar{2}), (102), (1\bar{1}3), (10\bar{4})$, respectively [27]. It is also apparent from Figure 6 that crystallization of PTT at different temperatures (at least within the range studied) did not affect the positions of these characteristic peaks, indicating that the crystal modification of PTT did not change with varying T_c. Desborough *et al.* [28] determined the crystal unit cell of PTT based on their WAXD results to be triclinic with axes a = 4.64 Å, b = 6.27 Å and c = 18.64 Å, and angles α = 98°, β = 90°, and γ = 112°, with an antichiral packing of molecules only along the c-axis. The space group proposed for this crystal modification was $P\bar{1}$ [28].

Apart from the information regarding the crystal modification, the sharpness and broadness of the characteristic peaks shown in Figure 6 also suggested, within the T_c range studied, that the apparent degree of crystallinity was an increase function with the crystallization temperature. Quantitatively, the apparent degree of crystallinity χ_c^{WAXD} can be calculated from the relative ratio of the integrated intensities under the crystalline peaks A_c to the integrated total intensities A_t, according to the following equation:

$$\chi_c^{WAXD} = \frac{A_c}{A_t} = \frac{A_c}{A_c + A_a} \in [0,1] \qquad (10)$$

where A_a is the integrated intensities of the amorphous halo. Figure 7 shows plot of the apparent degree of crystallinity of PTT samples isothermally crystallized at different temperatures (viz. the results were calculated from the raw WAXD patterns shown in Figure 6). According to Figure 7, the apparent degree of crystallinity of PTT was found to be ca. 18.1% when it was crystallized at 182°C, and it was found

to be ca. 28.4% at 206°C, which is agreeable with Chuah [3] who reported that the apparent degree of crystallinity of melt-crystallized PTT samples was in the range of 15 to 30%. As a result, it is qualitatively obvious that the WAXD degree of crystallinity of PTT increased with increasing crystallization temperature (at least within the T_c range studied).

4.9. Melting Behavior of PTT

Figure 8 shows subsequent DSC melting endotherms ($10^{\circ}C \cdot min^{-1}$) for PTT samples recorded after complete crystallization from the melt state at various crystallization temperatures ranging from 182 to 208°C. It is apparent that either double or triple melting endotherms were observed. At temperatures below ca. 194°C, triple melting endotherms were evident: the peaks were labeled as I, II, and III for low-, middle-, and high-temperature melting endotherm, respectively. According to Figure 8, it is apparent that the positions of both peaks I and II steadily increased with increasing crystallization temperature. However, the position of peak II was much less dependent on the crystallization temperature than that of peak I. With regards to peak III, evidence shown in Figure 8 clearly suggested that peak III disappeared altogether when the crystallization temperature was greater than ca. 194°C. Chung *et al.* [5] also reported the triple-melting phenomenon similar to what has been found in this work. They, however, attributed the occurrence of peak I to the recrystallization during the re-heating process and peaks II and III to the melting of the primary crystallites of two populations of the lamellar stacks [5].

In syndiotactic polypropylene (s-PP), triple melting endotherms were also observed in samples crystallized at "low" temperatures [19]. In s-PP, the three peaks were denoted the minor, the low-, and the high-temperature melting endotherms. The minor endotherm, located closed to the corresponding crystallization temperature, was postulated to be the melting of the secondary crystallites formed at T_c. The low-temperature melting endotherm was found to be the melting of the primary crystallites formed, and the high-temperature melting one was a result of the melting of the crystallites recrystallized during a heating scan. The triple-melting behavior observed in the subsequent melting of s-PP was, therefore, described as contributions from melting of the secondary crystallites and their recrystallization, partial melting of the

less stable fraction of the primary crystallites and their recrystallization, melting of the primary crystallites, and remelting of the recrystallized crystallites formed during the heating scan.

Based on the knowledge received on s-PP, we would like to postulate the origin for the triple melting endotherms for PTT, based on our observation. In the case of PTT, the occurrence of the minor endotherm, characterizing the melting of secondary crystallites, was not so apparent, even though trace amount of such a peak was observed in the heating scan for samples crystallized at "low" temperatures (i.e., ≤ 190°C). The occurrence of peak I was quite obvious, due to the fact that it became more pronounced and shifted towards a higher temperature with increasing crystallization temperature, suggesting that peak I was a result of the melting of the primary crystallites. On the contrary, peak II became less pronounced and its position was not shifted so much with increasing crystallization temperature, suggesting that peak II might be only a result of the melting of recrystallized crystallites during the heating scan. The occurrence of peak III was much less obvious, but it is logical at this point to postulate that peak III was a result of the melting of the recrystallized crystallites of different thicknesses which might become prevalent at low crystallization temperatures (i.e., ≤ 194°C). Detailed investigation on the multiple melting phenomenon in PTT is currently underway.

4.10. Determination of the Equilibrium Melting Temperatures

According to a theory derived by Hoffman and Weeks [24] (also known as the linear Hoffman-Weeks extrapolation, LHW), the equilibrium melting temperature T_m^o, that is the melting temperature of infinitely thick crystallites, can be estimated by linear extrapolation of the apparent melting temperature T_m versus the crystallization temperature T_c data to the line $T_m = T_c$. Mathematically, they arrived at the following equation:

$$T_m = \frac{T_c}{2\beta} + T_m^o\left[1 - \frac{1}{2\beta}\right] \qquad (11)$$

where β is the "thickening ratio." In other words, β indicates the ratio of the thickness of the mature crystallites L_c to that of the initial ones L_c*; therefore, $\beta = L_c/L_c$* is supposed to always be greater than or equal to 1. It should be noted that the

factor 2 in Equation (11) suggests that the thickness of the crystallites undergoing melting is approximately doubled that of the initial critical thickness [33].

Figure 9 shows a plot of the observed T_m versus T_c for PTT samples studied. It is evident that the observed T_m data displayed a linear relationship with T_c, at least within the temperature range of interest. The intersection of a least square line, fit to the data set for each sample, with the line $T_m = T_c$ provides the values of T_m^o. The slope of the least square line, which equals $1/2\beta$, can also be used to calculate the β parameter (i.e., $\beta = 0.5 \times \text{slope}^{-1}$). These values, along with the r^2 parameter, for each best fit are reported in Table 6. According to the LHW procedure, the T_m^o values for PET, PTT, and PBT were evaluated to be ca. 270.1, 243.6 and 235.4°C, respectively. Many researchers reported the T_m^o values for PET to be ca.280 [29] and 285°C [30], for PTT to be ca. 237 [31], 244 [32], 245 [33], and 248°C [2], and for PBT to be ca. 235 [30], 244 [26] and 245°C [31], respectively.

Although the non-linearity in the observed T_m-T_c data over a wide range of the temperature was explained to some extent by Alamo *et al.* [34], it is the recent contribution by Marand *et al.* [35] that offers a new extrapolative procedure to determine the T_m^o value of a semi-crystalline polymer based on the observed T_m-T_c data in which the observed T_m data were taken from samples crystallized at different temperatures but with the same *a priori* lamellar thickening coefficient. Derived based on the Gibbs-Thomson equation [24,36] and on the proposition of Lauritzen and Passaglia [37] on stem length fluctuation during chain folding, Marand *et al.* [35] proposed a new mathematical derivation which states a relationship between the observed melting temperature and the corresponding crystallization temperature. This equation is hereafter called the non-linear Hoffmann-Weeks extrapolation (NLHW), and is given in the form:

$$\frac{T_m^o}{T_m^o - T_m} = \beta^m \frac{\sigma_e^1}{\sigma_e^{GT}} \left[\frac{T_m^o}{T_m^o - T_c} + \frac{D_2 \Delta H_f^o}{2\sigma_e^1} \right] \qquad (12)$$

or in a simpler form:

$$M = \beta^m \frac{\sigma_e^1}{\sigma_e^{GT}} (X + a) \qquad (13)$$

where β^m is the thickening coefficient, σ_e^{GT} is the basal interfacial free energy associated with nuclei of critical size including the extra lateral surface energy due to fold protrusion and the mixing entropy associated with stems of different lengths (σ_e^{GT} is the basal interfacial free energy as appeared in the Gibbs-Thomson equation [24,36]), σ_e^{l} is the interfacial energy associated with the formation of the basal plane of the initial crystals which can be estimated from the slope of a plot of the lamellar thickness versus the inversed degree of undercooling (i.e., l_c^* versus ΔT^{-1}), D_2 is a constant, and all other parameters are the same as previously defined. It is worth nothing that, for most cases, it is safe to assume that $\sigma_e^{l} \approx \sigma_e^{GT}$ [35].

In order to apply Equation (13) to analyze the observed T_m-T_c data in real polymer systems, it is required that the observed T_m data be collected from samples crystallized at different temperatures but having the same lamellar thickening coefficient β^m for each set of the observed T_m-T_c data, corresponding values of M and X in Equation (13) can be calculated for a given choice of T_m^o value. In the case where $\sigma_e^{l} = \sigma_e^{GT}$, the "actual" equilibrium melting temperature T_m^o is taken as the seed T_m^o value which results in the plot of M versus X being a straight line with slope of unity (i.e. $\beta = 1$) and the intercept of a (i.e., $a = D_2\Delta H_f^o/2\sigma_e^{l}$). Figure 10 shows the evolution of the M versus X plots for different choices of seed T_m^o value for PTT. According to the NLHW procedure, the T_m^o values for PET, PTT, and PBT were evaluated to be ca. 323.9, 277.6 and 262.3°C, respectively. Wu and Woo [33] reported the T_m^o value for PTT based on the NLHW procedure to be ca. 273°C, which is in excellent agreement with our result. The marked difference in the T_m^o values obtained by the LHW and the NLHW procedure should be noted.

5. CONCLUSIONS

In this manuscript, DSC was used to investigate the overall kinetics of melt-crystallization of three different linear aromatic polyesters, namely PET, PTT, and PBT, under isothermal quiescent conditions and subsequent melting behavior. A non-linear multi-variable regression program was used to fit the experimental data obtained for each polymer at different crystallization temperatures to four different macrokinetic models, namely the Avrami, Tobin, Malkin, and Urbanovici-Segal

models. The crystallization kinetic parameters specific to each model were obtained along with the best fits, provided by the program. It is was found that the quality of each model, judged by comparing the values of the r^2 parameter, in describing the isothermal crystallization data of these polyesters was in the following order: the Urbanovici-Segal, Avrami, Malkin, and Tobin models.

All of the crystallization rate parameters (i.e., $t_{0.5}^{-1}$, K_a, K_t, C_1 and K_{us}) were found to be very sensitive to changes in the crystallization temperature. Within the crystallization temperature range studied (i.e., $182 \leq T_c \leq 208$ °C), the values of the rate parameters for these polyesters were all found to increase with decreasing temperature (or with increasing degree of undercooling), suggesting that these polyesters crystallized faster at low temperatures than that at high temperatures. It was also shown that all of the bulk crystallization rate parameters (i.e., $t_{0.5}^{-1}$, K_a, K_t, C_1 and K_{us}) have a finite, definable relationship with the crystallization temperature T_c (or, to be exact, the degree of undercooling ΔT), in which they can be described based on an equation similar to that proposed by Hoffman *et al.* [24,25] for the temperature-dependence characteristic of the linear crystal growth rate of semi-crystalline polymers.

WAXD patterns obtained for PTT samples crystallized in the temperature range of 182 to 206°C showed seven characteristic peaks at the scattering angles 2θ of ca. 15.3, 16.8, 19.4, 21.8, 23.6, 24.6, and 27.3°, corresponding to the reflection planes of $(010), (0\bar{1}2), (012), (10\bar{2}), (102), (1\bar{1}3), (10\bar{4})$, respectively. Changes in the crystallization temperature did not affect the diffraction pattern, suggesting that the crystal modification did not change with changes in the crystallization temperature (at least within the temperature range studied). The apparent degree of crystallinity χ_c^{WAXD} of these samples was also calculated and was found to be an increasing function with increasing crystallization temperature (i.e., from ca. 18.1% at T_c = 182°C to 28.4% at T_c = 206°C).

The subsequent melting endotherms for PTT samples isothermally crystallized at temperatures ranging from 182 to 208°C exhibited either triple (at temperatures lower than ca. 194°C) or double (at temperatures greater than ca. 194°C) melting phenomenon. These peaks were denoted peaks I, II, and III for low-,

middle-, and high-temperature melting endotherm, respectively. For triple melting phenomenon, it was postulated that the occurrence of peak I was a result of the melting of the primary crystallites, peak II was a result of the melting of recrystallized crystallites, and peak III was a result of the melting of the recrystallized crystallites of different stabilities.

Lastly, analysis of the melting temperature of the primary crystallites according to the linear and non-linear Hoffman-Weeks extrapolative methods to obtain the equilibrium melting temperatures T_m^o of these polyesters was conducted. According to the linear Hoffman-Weeks extrapolation, the T_m^o values for PET, PTT, and PBT were found to be ca. 270.1, 243.6 and 235.4°C, respectively. According to the non-linear Hoffman-Weeks extrapolation, a much higher values of ca. 323.9, 277.6 and 262.3°C were instead obtained.

6. ACKNOWLEDGMENTS

The authors wish to thank Dr. Hoe H. Chuah and his co-workers of Shell Chemical Company (USA), Ltd. for supply of PTT and for their kind assistance on molecular weight measurements on all of the polyester resins received, Dr. Gi-Dae Choi and Soo-Min Lee of LG Chem (Korea) Ltd. for supply of PBT, and Indo PET (Thailand) Ltd. for supply of PET. PS acknowledges a grant provided by Chulalongkorn University through the Development Grants for New Faculty/Researchers. Partial support from the Petroleum and Petrochemical Technology Consortium and the Petroleum and Petrochemical College is greatly acknowledged.

REFERENCES

[1] Whinfield JR and Dickson JT, Brit Pat 578,079 (June 14, 1946).

[2] Huang JM and Chang FC, J Polym Sci – Polym Phys 2000, 38, 934.

[3] Chuah H, in John Scheirs and Timothy Long ed. "Modern Polyester," John Wiley & Sons, New York.

[4] Chuah H, Polym Engng Sci 2001, 41, 308.

[5] Chung WT, Yeh WJ, and Hong PD, J Appl Polym Sci 2002, 83, 2426.

[6] Hay JN and Sabir M, Polymer 1969, 10, 203.

[7] Hay JN, Brit Polym J 1979, 11, 137.

[8] Kolmogorov AN, Izvestiya Akad USSR, Ser Math 1937, 1, 355.

[9] Johnson WA and Mehl KF, Trans Am Inst Mining Met Eng 1939, 135, 416.

[10] Avrami M, J Chem Phys 1939, 7, 1103.

[11] Avrami M, J Chem Phys 1940, 8, 212.

[12] Avrami M, J Chem Phys 1941, 9, 177.

[13] Evans UR, Trans Faraday Soc 1945, 41, 365.

[14] Tobin MC, J Polym Sci – Polym Phys 1974, 12, 399.

[15] Tobin MC, J Polym Sci – Polym Phys 1976, 14, 2253.

[16] Tobin MC, J Polym Sci – Polym Phys 1977, 15, 2269.

[17] Malkin AY, Beghishev VP, Keapin IA, and Bolgov SA, Polym Engng Sci 1984, 24, 1396.

[18] Urbanovici E and Segal E, Thermochim Acta 1990, 171, 87.

[19] Supaphol P and Spruiell JE, Polymer 2001, 42, 699.

[20] Wunderlich B, In "Macromolecular Physics," Vol. 2, Academic Press, New York, 1976, 132.

[21] Janeschitz-Kriegl H, Ratajski E, and Wipel H, Colloid Polym Sci 1999, 227, 217.

[22] Supaphol P, Thermochim Acta 2001, 370, 37.

[23] Supaphol P, and Spruiell JE, J Macromol Sci – Phys 2000, 39, 257.

[24] Hoffman JD, Davis GT, Lauritzen JI Jr, in: N.B. Hannay (Ed.), "Treatise on Solid State Chemistry, Vol. 3, Plenum Press, New York, 1976, Chapter 7.

[25] Hoffman JD and Miller RL, Polymer 1997, 38, 3151.

[26] Runt J, Miley DM, Zhang X, Gallangher KP, McFeathers K, and Fishburn J, Macromolecules 1992, 25, 1929.

[27] Wang B, Li YC, Hanzlicek J, Cheng SZD, Gail PH, Grebowicz J, and Ho RM, Polymer 2001, 42, 7171.

[28] Desborough IJ, Hall IH, and Neisser JZ, Polymer 1979, 20, 419.

[29] Phillips PJ and Tseng HT, Macromolecules 1989, 22, 1649.

[30] Wunderlich B, in "Thermal Analysis," Academic Press, New York, 1990.

[31] Pyda M, Boller A, Grebowicz J, Chuah H, Lebedev BV, and Wunderlich B, J Polym Sci – Polym Phys 1998, 36, 2499.

[32] Kim YH, Kim KJ, and Lee KM, J Korean Fiber Soc 1997, 34, 860.

[33] Wu P-L and Woo EM, J Polym Sci – Polym Phys 2002, 40, 1571.

[34] Alamo RG, Viers BD, and Mandelkern L, Macromolecules 1995, 28, 3205.

[35] Marand H, Xu J, and Srinivas S, Macromolecules 1998, 31, 8219.

[36] Brown RG and Eby RK, J Appl Phys 1964, 35, 1156.

[37] Lauritzen JI and Passaglia E, J Res Natl Bur Stand 1967, 71, 261.

CAPTIONS OF TABLES

Table 1 Overall crystallization kinetic data for PET, PTT, and PBT based on the Avrami model

Table 2 Overall crystallization kinetic data for PET, PTT, and PBT based on the Tobin model

Table 3 Overall crystallization kinetic data for PET, PTT, and PBT based on the Malkin model

Table 4 Overall crystallization kinetic data for PET, PTT, and PBT based on the Urbanovici-Segal model

Table 5 Fitting parameters for the best possible fits of the respective rate parameters of PET, PTT, and PBT according to Equation (9)

Table 6 Estimated equilibrium melting temperatures for PET, PTT, and PBT according to linear and non-linear Hoffman-Week extrapolations, along with other fitting parameters

CAPTIONS OF FIGURES

Figure 1 Relative crystallinity as a function of time of PTT for two crystallization temperatures .

Figure 2 Half-time of crystallization $t_{0.5}$ as a function of degree of undercooling for PET, PTT, and PBT.

Figure 3 Reciprocal half-time of crystallization $t_{0.5}^{-1}$ as a function of degree of undercooling for PET, PTT, and PBT.

Figure 4 Respective exponent of time specific to the Avrami, Tobin, Malkin, and Urbanovici-Segal mocrokinetic models, including the Urbanovici-Segal r parameter, as a function of crystallization temperature.

Figure 5 Respective kinetic rate of crystallization specific to the Avrami, Tobin, Malkin, and Urbanovici-Segal mocrokinetic models as a function of crystallization temperature. The experimental data, shown as various geometrical points, were fitted to Equation (9), and the best fits are shown as various lines.

Figure 6 Wide-angle X-ray diffractograms for PTT samples isothermally crystallized from the melt state at different crystallization temperatures.

Figure 7 Apparent degree of crystallinity for PTT samples (analyzed from the WAXD patterns) as a function of crystallization temperature.

Figure 8 Subsequent melting endotherms (recorded at $10^{\circ}C \cdot min^{-1}$) for PTT samples isothermally crystallized from the melt state at different crystallization temperatures. Peaks I, II, and III denotes the low-, middle-, and high-temperature melting endotherm, respectively.

Figure 9 Observed melting temperature of the primary crystallites as a function of crystallization temperature for PTT, shown along with the linear Hoffman-Weeks extrapolation (solid line) and the non-linear Hoffman-Weeks extrapolation (dotted line, calculated using $\beta^m = 1.00$ and $a = 1.02$).

Figure 10 Plots of the scaled observed melting temperature $M = T_m^{\circ}/(T_m^{\circ} - T_m)$ against the scaled crystallization temperature $X = T_m^{\circ}/(T_m^{\circ} - T_c)$ for various choice of the seeded equilibrium melting temperature T_m° for the observed T_m-T_c data of PTT.

Table 1 Overall crystallization kinetic data for PET, PTT, and PBT based on the Avrami model

	PET							PTT							PBT						
T_c	$t_{0.5}$	K_a^*	n_a	K_a	r^2	n_a^{**}	K_a^{**}	$t_{0.5}$	K_a^*	n_a	K_a	r^2	n_a^{**}	K_a^{**}	$t_{0.5}$	K_a^*	n_a	K_a	r^2	n_a^{**}	K_a^{**}
°C	min	min^{-1}		min^{-1}			min^{-1}	min	min^{-1}		min^{-1}			min^{-1}	min	min^{-1}		min^{-1}			min^{-1}
184	1.31	0.630	1.87	0.628	0.9999	1.90	0.629	0.58	1.44	2.03	1.46	0.9994	1.87	1.44	0.30	2.83	2.11	2.86	0.9996	1.87	2.83
186	1.39	0.597	2.00	0.603	0.9995	1.77	0.594	0.64	1.26	1.75	1.27	0.9998	1.74	1.27	0.38	2.21	2.15	2.24	0.9996	1.93	2.21
188	1.45	0.557	1.73	0.562	0.9993	1.60	0.555	0.72	1.15	1.98	1.16	0.9998	1.91	1.15	0.40	2.13	2.24	2.14	0.9997	2.03	2.12
190	1.45	0.582	2.17	0.590	0.9999	2.04	0.582	0.90	0.934	2.12	0.940	0.9999	2.07	0.934	0.53	1.58	2.05	1.60	0.9996	1.85	1.58
192	1.49	0.538	1.67	0.544	0.9988	1.55	0.535	1.05	0.791	1.96	0.792	0.9999	1.94	0.791	0.53	1.55	1.80	1.57	0.9994	1.58	1.55
194	1.56	0.518	1.74	0.522	0.9994	1.67	0.516	1.35	0.621	2.03	0.626	0.9998	1.95	0.621	0.78	1.07	2.01	1.08	0.9995	1.79	1.06
196	1.72	0.478	1.87	0.487	0.9990	1.69	0.476	1.57	0.544	2.29	0.549	0.9998	2.25	0.515	0.88	0.911	1.65	0.920	0.9993	1.44	0.904
198	1.98	0.410	1.74	0.414	0.9988	1.63	0.408	2.16	0.386	2.00	0.387	0.9999	2.03	0.388	1.27	0.631	1.63	0.636	0.9993	1.42	0.625
200	2.26	0.352	1.59	0.355	0.9990	1.49	0.351	2.97	0.289	2.40	0.294	0.9992	2.26	0.290	1.53	0.542	1.95	0.547	0.9995	1.72	0.537
202	2.57	0.326	2.05	0.330	0.9997	1.91	0.325	3.69	0.228	2.12	0.228	0.9996	2.08	0.227	2.66	0.308	1.82	0.312	0.9992	1.60	0.305
204	2.84	0.288	1.83	0.302	0.9967	1.80	0.299	4.95	0.172	2.27	0.172	0.9996	2.28	0.173	3.65	0.219	1.63	0.219	0.9970	1.58	0.215
205	2.97	0.275	1.82	0.276	0.9997	1.84	0.278	5.93	0.145	2.39	0.147	0.9993	2.24	0.145	-	-	-	-	-	-	-
206	2.98	0.276	1.86	0.282	0.9972	1.71	0.276	6.61	0.129	2.24	0.129	0.9998	2.24	0.129	4.76	0.169	1.66	0.170	0.9912	1.64	0.170
207	3.29	0.249	1.84	0.249	0.9998	1.84	0.250	-	-	-	-	-	-	-	-	-	-	-	-	-	-
208	3.99	0.207	1.91	0.210	0.9980	1.84	0.206	7.60	0.113	2.39	0.114	0.9989	2.24	0.114	7.46	0.110	1.85	0.113	0.9971	1.69	0.109
215	4.71	0.176	1.97	0.173	0.9991	2.11	0.175	-	-	-	-	-	-	-	-	-	-	-	-	-	-
220	10.2	0.082	2.05	0.082	0.9992	2.15	0.096	-	-	-	-	-	-	-	-	-	-	-	-	-	-

Table 2 Overall crystallization kinetic data for PET, PTT, and PBT based on the Tobin model

	PET					PTT					PBT				
T_c	$t_{0.5}$	n_t	K_t	r^2	K_t^*	$t_{0.5}$	n_t	K_t	r^2	K_t^*	$t_{0.5}$	n_t	K_t	r^2	K_t^*
°C	min		min^{-1}		min^{-1}	min		min^{-1}		min^{-1}	min		min^{-1}		min^{-1}
184	1.13	2.81	0.914	0.9913	0.885	0.58	3.43	1.79	0.9919	1.72	0.30	3.66	3.48	0.9939	3.37
186	1.39	3.47	0.737	0.9927	0.717	0.64	3.06	1.60	0.9943	1.56	0.38	3.70	2.70	0.9938	2.63
188	1.45	2.83	0.714	0.9901	0.688	0.72	3.35	1.42	0.9937	1.39	0.40	3.85	2.58	0.9942	2.51
190	1.45	3.41	0.717	0.9922	0.689	0.90	3.57	1.01	0.9940	1.11	0.53	3.64	1.95	0.9935	1.89
192	1.49	2.69	0.697	0.9885	0.670	1.05	3.18	0.982	0.9946	0.953	0.53	3.28	1.94	0.9918	1.91
194	1.56	2.81	0.662	0.9907	0.639	1.35	3.34	0.770	0.9936	0.743	0.78	3.45	1.32	0.9927	1.28
196	1.72	3.07	0.608	0.9895	0.582	1.57	3.62	0.661	0.9941	0.639	0.88	2.97	1.16	0.9904	1.14
198	1.98	2.79	0.528	0.9888	0.506	2.16	3.30	0.478	0.9958	0.464	1.27	2.90	0.808	0.9899	0.790
200	2.26	2.55	0.460	0.9889	0.443	2.97	3.65	0.352	0.9915	0.337	1.53	3.35	0.674	0.9921	0.654
202	2.57	3.34	0.405	0.9926	0.390	3.69	3.16	0.281	0.9929	0.271	2.66	3.04	0.389	0.9905	0.377
204	2.84	2.82	0.386	0.9846	0.352	4.95	3.78	0.209	0.9955	0.202	3.65	2.46	0.283	0.9863	0.274
205	2.97	2.92	0.346	0.9958	0.337	5.93	3.68	0.176	0.9922	0.169	-	-	-	-	-
206	2.98	2.82	0.355	0.9856	0.336	6.61	3.51	0.157	0.9948	0.151	4.76	2.56	0.216	0.9925	0.210
207	3.29	2.92	0.313	0.9941	0.304	-	-	-	-	-	-	-	-	-	-
208	3.99	2.81	0.262	0.9881	0.251	7.60	3.65	0.136	0.9916	0.132	7.46	2.78	0.142	0.9899	0.134
215	4.71	2.87	0.218	0.9927	0.212	-	-	-	-	-	-	-	-	-	-
220	10.2	3.12	0.099	0.9921	0.098	-	-	-	-	-	-	-	-	-	-

Table 3 Overall crystallization kinetic data for PET, PTT, and PBT based on the Malkin model

	PET						PTT						PBT					
T_c °C	$t_{0.5}$ min	C_0	C_1 min^{-1}	r^2	C_0^*	C_1^* min^{-1}	$t_{0.5}$ min	C_0	C_1 min^{-1}	r^2	C_1^*	C_2^* min^{-1}	$t_{0.5}$ min	C_0	C_1 min^{-1}	r^2	C_1^*	C_2^* min^{-1}
184	1.13	5.95	1.82	0.9997	6.27	1.88	0.58	13.3	4.72	0.9994	12.7	4.69	0.297	13.3	9.25	0.9998	14.6	9.56
186	1.39	10.7	1.84	0.9997	12.0	1.91	0.64	7.01	3.41	0.9997	7.30	3.50	0.381	14.56	7.42	0.9998	15.7	7.62
188	1.45	6.49	1.47	0.9995	7.00	1.53	0.72	12.0	3.63	0.9995	11.6	3.62	0.399	17.39	7.48	0.9998	18.3	7.60
190	1.45	17.5	2.05	0.9994	16.3	2.70	0.90	17.4	3.28	0.9994	14.9	3.16	0.528	12.22	5.06	0.9998	13.2	5.21
192	1.49	5.71	1.37	0.9990	6.13	1.42	1.05	11.5	2.46	0.9997	11.1	2.46	0.525	6.82	4.18	0.9997	8.13	4.45
194	1.56	7.20	1.41	0.9993	7.16	1.43	1.35	13.7	2.04	0.9997	12.7	2.02	0.779	10.93	3.31	0.9997	12.2	3.44
196	1.72	9.02	1.41	0.9992	9.36	1.44	1.57	23.8	2.07	0.9995	19.9	1.99	0.879	4.86	2.20	0.9997	5.85	2.37
198	1.98	7.10	1.12	0.9989	7.16	1.13	2.16	11.7	1.21	0.9995	12.0	1.23	1.27	4.56	1.50	0.9997	5.58	1.61
200	2.26	4.55	0.870	0.9993	5.06	0.872	2.97	28.0	1.15	0.9998	23.9	1.11	1.53	9.67	1.62	0.9997	10.9	1.69
202	2.57	13.5	1.07	0.9997	13.1	1.07	3.69	16.3	0.780	0.9989	14.9	0.766	2.66	7.28	0.846	0.9997	8.47	0.896
204	2.84	14.0	0.960	0.9973	8.64	0.873	4.95	22.2	0.644	0.9996	19.3	0.620	3.65	5.93	0.558	0.9971	5.58	0.556
205	2.97	8.25	0.780	0.9994	8.47	0.793	5.93	27.7	0.575	0.9986	23.5	0.554	-	-	-	-	-	-
206	2.98	9.61	0.832	0.9975	9.18	0.829	6.61	19.4	0.463	0.9994	18.3	0.458	4.76	5.57	0.425	0.9986	5.99	0.440
207	3.29	8.96	0.721	0.9995	8.82	0.725	-	-	-	-	-	-	-	-	-	-	-	-
208	3.99	11.3	0.643	0.9977	10.1	0.634	7.60	26.5	0.444	0.9991	23.5	0.432	7.46	8.70	0.321	0.9980	9.00	0.331
215	4.71	11.6	0.539	0.9981	11.3	0.541	-	-	-	-	-	-	-	-	-	-	-	-
220	10.2	13.5	0.266	0.9910	13.1	0.265	-	-	-	-	-	-	-	-	-	-	-	-

Table 4 Overall crystallization kinetic data for PET, PTT, and PBT based on the Urbanovici-Segal model

	PET						PTT						PBT					
T_c °C	$t_{0.5}$ min	n_{us}	K_{us} min^{-1}	K_{us}^* min^{-1}	r	r^2	$t_{0.5}$ min	n_{us}	K_{us} min^{-1}	K_{us}^* min^{-1}	r	r^2	$t_{0.5}$ min	n_{us}	K_{us} min^{-1}	K_{us}^* min^{-1}	r	r^2
184	1.31	1.91	0.634	0.636	1.03	0.9999	0.58	2.05	1.41	1.43	0.93	0.9996	0.297	2.12	2.81	2.82	0.97	0.9997
186	1.39	2.03	0.621	0.602	1.03	0.9987	0.64	1.78	1.29	1.28	1.04	0.9989	0.381	2.13	2.19	2.19	0.95	0.9998
188	1.45	1.67	0.533	0.540	0.89	0.9998	0.72	1.88	1.12	1.12	0.92	0.9999	0.399	2.21	2.17	2.12	0.99	0.9995
190	1.45	2.17	0.304	0.580	0.94	0.9996	0.90	2.08	0.931	0.926	0.97	0.9999	0.528	2.05	1.60	1.59	1.01	0.9996
192	1.49	1.67	0.520	0.526	0.89	0.9992	1.05	1.92	0.783	0.782	0.96	0.9999	0.525	1.92	1.59	1.59	1.04	0.9992
194	1.56	1.74	0.506	0.510	0.93	0.9995	1.35	1.89	0.602	0.599	0.88	0.9999	0.779	2.02	1.09	1.07	1.01	0.9991
196	1.72	1.87	0.470	0.472	0.93	0.9931	1.57	2.16	0.527	0.528	0.87	0.9999	0.879	1.68	0.931	0.915	1.00	0.9989
198	1.98	1.75	0.398	0.401	0.89	0.9992	2.16	2.10	0.397	0.396	1.10	0.9999	1.27	1.66	0.659	0.636	1.02	0.9981
200	2.26	1.60	0.346	0.347	0.93	0.9993	2.97	2.33	0.293	0.286	0.95	0.9991	1.53	1.95	0.539	0.538	0.96	0.9996
202	2.57	1.83	0.311	0.310	0.84	0.9999	3.69	1.91	0.214	0.216	0.80	0.9998	2.66	1.86	0.316	0.310	1.02	0.9989
204	2.84	1.81	0.297	0.281	0.89	0.9983	4.95	2.35	0.177	0.175	1.09	0.9996	3.65	1.70	0.225	0.223	1.04	0.9963
205	2.97	1.86	0.281	0.280	1.07	0.9998	5.93	2.17	0.139	0.138	0.81	0.9997	-	-	-	-	-	-
206	2.98	1.68	0.253	0.255	0.72	0.9994	6.61	2.27	0.130	0.129	1.03	0.9998	4.76	1.59	0.164	0.164	0.91	0.9992
207	3.29	1.80	0.245	0.245	0.94	0.9999	-	-	-	-	-	-	-	-	-	-	-	-
208	3.99	1.92	0.203	0.204	0.92	0.9986	7.60	2.40	0.115	0.113	1.01	0.9989	7.46	1.50	0.095	0.096	0.58	0.9997
215	4.71	1.77	0.162	0.166	0.80	0.9993	-	-	-	-	-	-	-	-	-	-	-	-
220	10.2	1.83	0.076	0.077	0.79	0.9997	-	-	-	-	-	-	-	-	-	-	-	-

Table 5 Fitting parameters for the best possible fits of the respective rate parameters of PET, PTT, and PBT according to Equation (9)

PET					PTT					PBT				
C(K)	ψ_0	A(cal mol^{-1})	B(K^2)	r^2	C(K)	ψ_0	A(cal mol^{-1})	B(K^2)	r^2	C(K)	ψ_0	A(cal mol^{-1})	B(K^2)	r^2
$t_{0.5}^{-1}$(min^{-1})					$t_{0.5}^{-1}$(min^{-1})					$t_{0.5}^{-1}$(min^{-1})				
30	1.29X10^8	2687	3.25X10^5	0.9626	30	1.11X10^7	2684	1.97X10^5	0.9964	30	4.73X10^4	1500	1.20X10^5	0.9722
50	1.23X10^8	3215	3.07X10^5	0.9566	50	5.75X10^7	3544	2.02X10^5	0.9964	50	2.55X10^4	1500	1.15X10^5	0.9725
K_a(min^{-1})					K_a(min^{-1})					K_a(min^{-1})				
30	6.33X10^7	2590	3.19X10^5	0.9341	30	2.37X10^6	2348	1.88X10^5	0.9964	30	4.70X10^4	1500	1.23X10^5	0.9776
50	1.48X10^5	1866	2.28X10^5	0.9017	50	2.80X10^4	1398	1.57X10^5	0.9958	50	2.53X10^4	1500	1.19X10^5	0.9775
K_t(min^{-1})					K_t(min^{-1})					K_t(min^{-1})				
30	9.09X10^7	2640	3.18X10^5	0.9578	30	1.22X10^5	1500	1.71X10^5	0.9831	30	5.07X10^4	1500	1.21X10^5	0.9737
50	8.98X10^7	3164	3.01X10^5	0.9512	50	5.75X10^4	1500	1.64X10^5	0.9832	50	2.73X10^4	1500	1.16X10^5	0.9740
C_1(min^{-1})					C_1(min^{-1})					C_1(min^{-1})				
30	1.52X10^8	1647	2.72X10^5	0.8059	30	1.50X10^5	1500	1.53X10^5	0.9276	30	7.78X10^5	1708	1.45X10^5	0.9543
50	6.57X10^8	2269	2.80X10^5	0.8062	50	7.09X10^4	1500	1.46X10^5	0.9277	50	3.18X10^5	1648	1.40X10^5	0.9568
K_{us}(min^{-1})					K_{us}(min^{-1})					K_{us}(min^{-1})				
30	6.08X10^7	2621	3.16X10^5	0.9195	30	1.38X10^7	2801	1.99X10^5	0.9969	30	3.96X10^4	1500	1.20X10^5	0.9716
50	1.75X10^5	1946	2.27X10^5	0.8839	50	5.30X10^4	1589	1.61X10^7	0.996	50	2.13X10^4	1500	1.15X10^5	0.9717

Table 6 Estimated equilibrium melting temperatures for PET, PTT, and PBT according to linear and non-linear Hoffman-Week extrapolations, along with other fitting parameters

Polymer	LHW				NLHW			
	T_m^o(°C)	Slope	β	r^2	T_m^o(°C)	β^m	a	r^2
PET	270.1	0.45	1.11	0.9932	323.9	1.00	1.17	0.9971
PTT	243.6	0.60	0.82	0.9988	277.6	1.00	1.02	0.9979
PBT	235.4	0.54	0.92	0.9826	262.3	1.00	1.47	0.9946

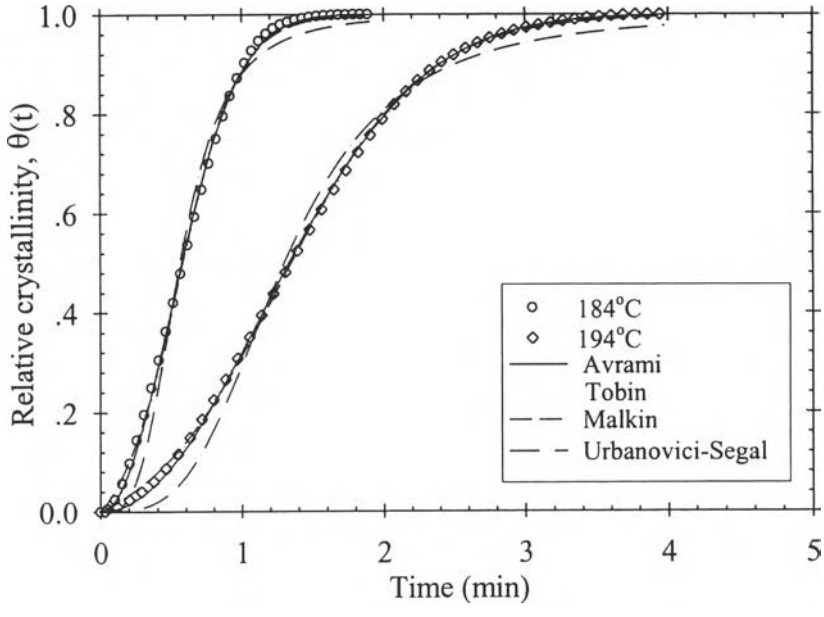
1.0
.8
.6
.4
.2
0.0
Relative crystallinity, θ(t)
0
1
2
3
4
5
Time (min)
184°C
194°C
Avrami
Tobin
Malkin
Urbanovici-Segal

Figure 1

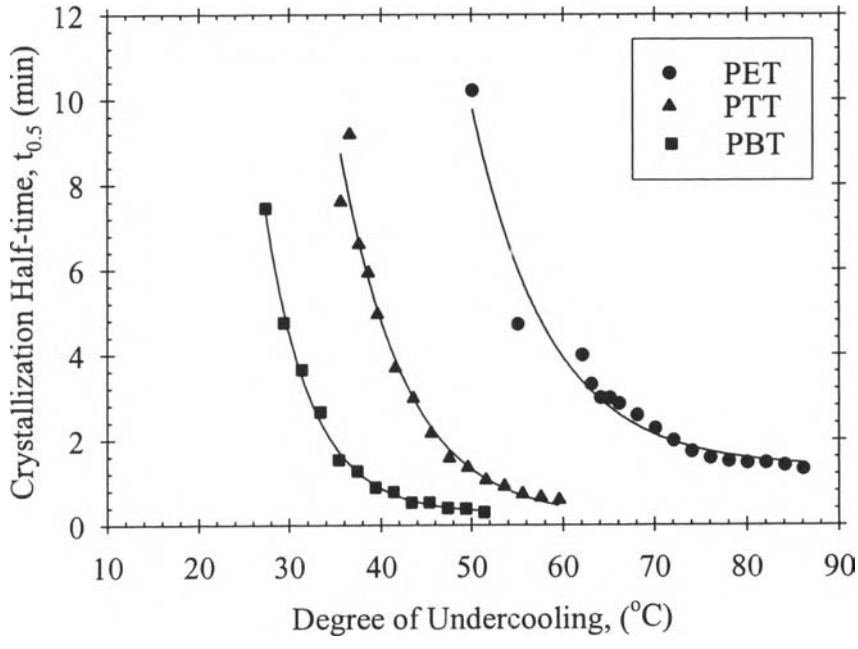
PET
PTT
PBT
Crystallization Half-time, $t_{0.5}$ (min)
Degree of Undercooling, (°C)
0
2
4
6
8
10
12
10
20
30
40
50
60
70
80
90

Figure 2

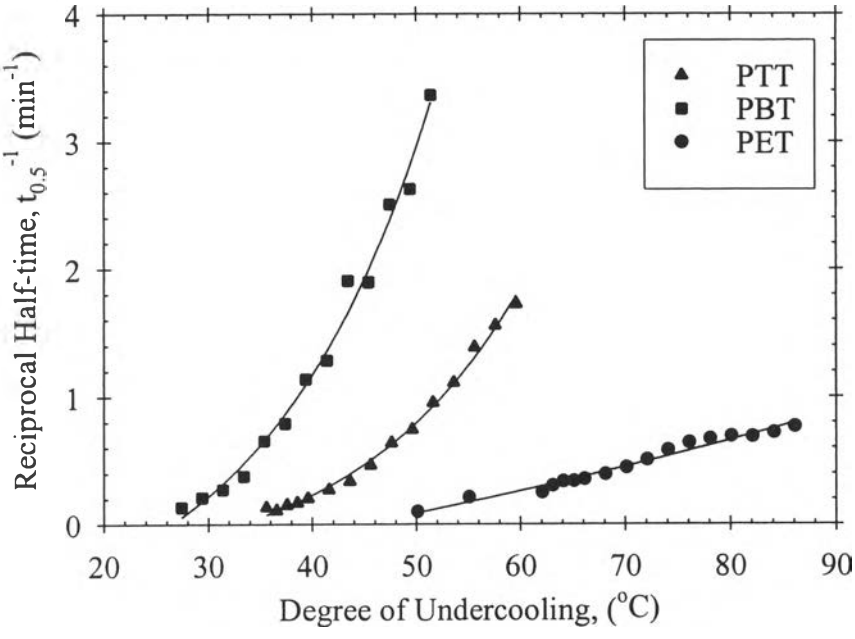
PTT
PBT
PET
Reciprocal Half-time, $t_{0.5}^{-1}$ (min^{-1})
Degree of Undercooling, (°C)
0
1
2
3
4
20
30
40
50
60
70
80
90

Figure 3

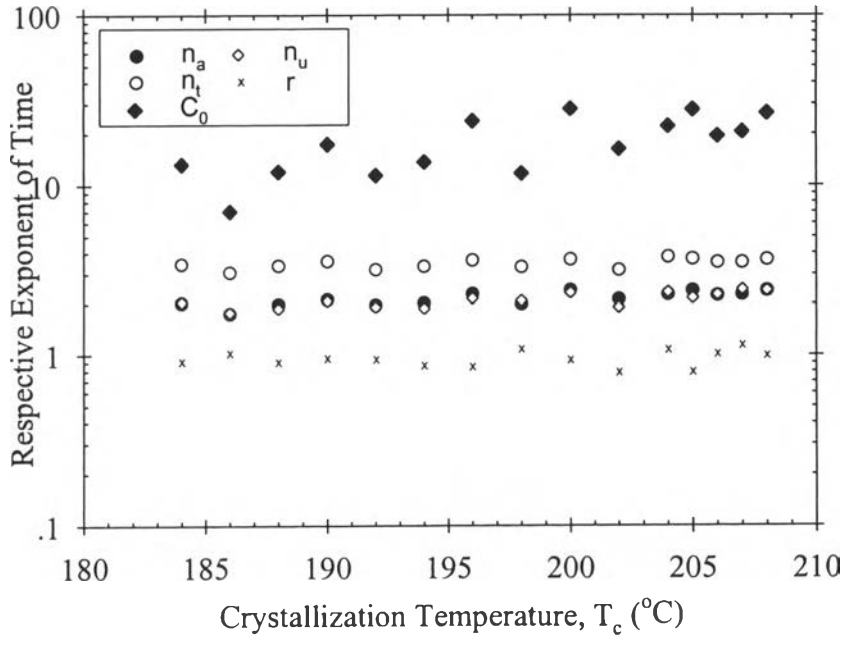
100
10
1
.1
Respective Exponent of Time
n_a
n_u
n_t
r
C_0
180
185
190
195
200
205
210
Crystallization Temperature, T_c (°C)

Figure 4

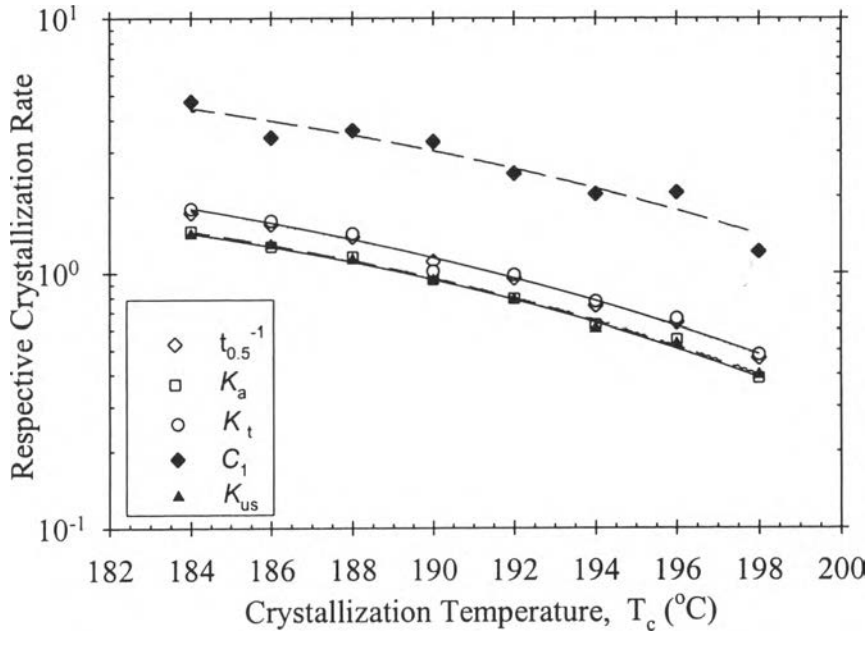
Respective Crystallization Rate
10^1
10^0
10^{-1}
$t_{0.5}^{-1}$
K_a
K_t
C_1
K_{us}
182 184 186 188 190 192 194 196 198 200
Crystallization Temperature, T_c (°C)

Figure 5

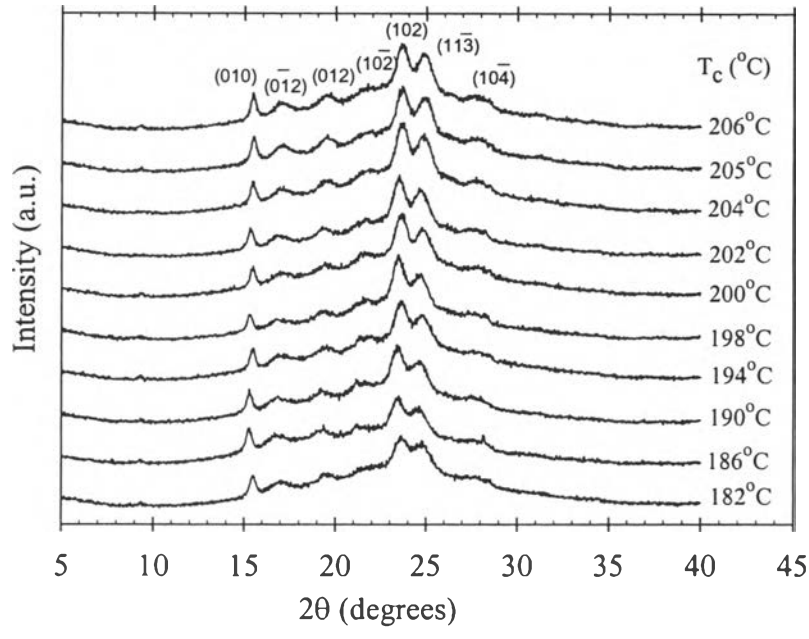
(010)
(01$\bar{2}$)
(012)
(10$\bar{2}$)
(102)
(11$\bar{3}$)
(10$\bar{4}$)
T_c (°C)
206°C
205°C
204°C
202°C
200°C
198°C
194°C
190°C
186°C
182°C
Intensity (a.u.)
5
10
15
20
25
30
35
40
45
2θ (degrees)

Figure 6

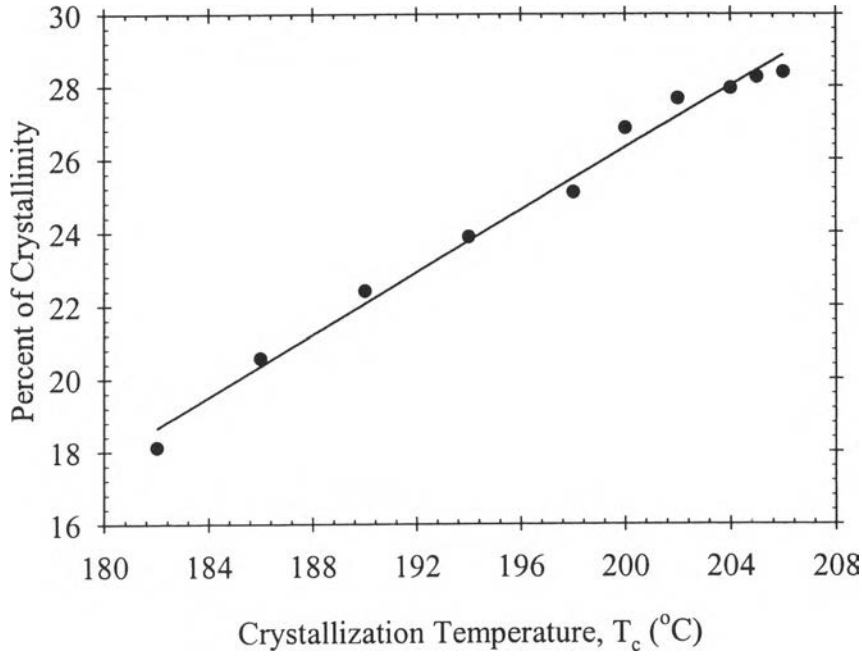
Percent of Crystallinity
30
28
26
24
22
20
18
16
180
184
188
192
196
200
204
208
Crystallization Temperature, T_c (^{o}C)

Figure 7

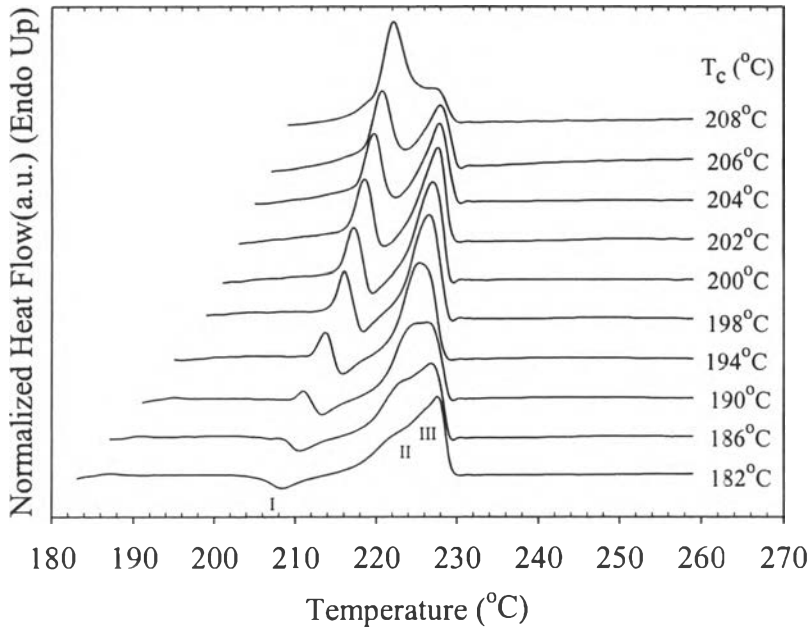
Normalized Heat Flow(a.u.) (Endo Up)
T_c (°C)
208°C
206°C
204°C
202°C
200°C
198°C
194°C
190°C
186°C
182°C
I
II
III
180 190 200 210 220 230 240 250 260 270
Temperature (°C)

Figure 8

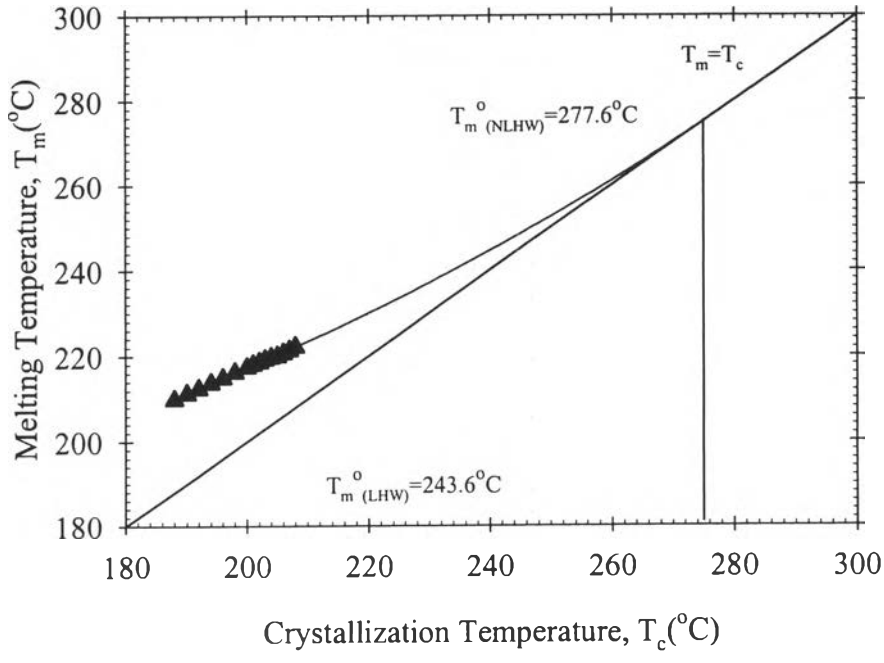
300
280
260
240
220
200
180
180
200
220
240
260
280
300
Melting Temperature, T_m(°C)
Crystallization Temperature, T_c(°C)
T_m=T_c
T_m^o (NLHW)=277.6°C
T_m^o (LHW)=243.6°C

Figure 9

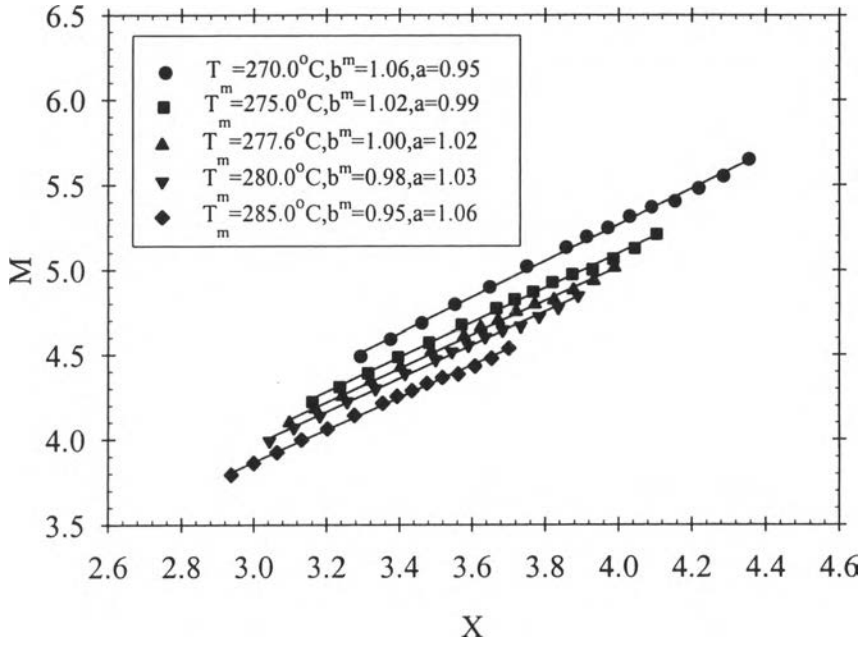
T =270.0°C,b^m=1.06,a=0.95
T^m=275.0°C,b^m=1.02,a=0.99
T^m=277.6°C,b^m=1.00,a=1.02
T^m=280.0°C,b^m=0.98,a=1.03
T^m=285.0°C,b^m=0.95,a=1.06
m
M
X
6.5
6.0
5.5
5.0
4.5
4.0
3.5
2.6
2.8
3.0
3.2
3.4
3.6
3.8
4.0
4.2
4.4
4.6

Figure 10